Silver nanoparticles/graphene oxide decorated carbon fiber synergistic reinforcement in epoxy-based composites

Caifeng Wang [a, b], Min Zhao [b, c, d], Jun Li [b], Jiali Yu [b], Shaofan Sun [b], Shengsong Ge [e], Xingkui Guo [e], Fei Xie [b], Bo Jiang [b, f], Evan K. Wujcik [g], Yudong Huang [b, *], Ning Wang [c, **], Zhanhu Guo [d, ***]

[a] College of Chemistry, Chemical Engineering and Environmental Engineering, Liaoning Shihua University, Fushun 113001, China
[b] MIIT Key Laboratory of Critical Materials Technology for New Energy Conversion and Storage, School of Chemistry and Chemical Engineering, Harbin Institute of Technology, Harbin 150001, China
[c] Engineered Multifunctional Composites (EMC) Nanotechnology LLC, Knoxville, TN 37934, USA
[d] Integrated Composites Laboratory (ICL), Department of Chemical and Biomolecular Engineering, University of Tennessee (UT), Knoxville, TN 37996, USA
[e] College of Chemical and Environmental Engineering, Shandong University of Science and Technology, Qingdao 266590, China
[f] State Key Laboratory for Modification of Chemical Fibers and Polymer Materials, Donghua University, Shanghai 200000, China
[g] Materials Engineering and Nanosensor [MEAN] Laboratory, Department of Chemical and Biological Engineering, The University of Alabama, Tuscaloosa, AL, USA

ARTICLE INFO

ABSTRACT

A novel two-layer reinforced carbon fiber (CF), i.e., Ag nanoparticles (Ag NPs)/graphene oxide (GO) reinforced CF (named as CF/Ag/GO) was prepared by an electrochemical deposition and electrophoretic deposition (EPD) consequently. The modified fiber showed an increased interfacial shear strength (IFSS) and tensile strength. Transmission electron microscopy (TEM), scanning electron microscopy (SEM), Fourier transform infrared spectra (FTIR), X-ray photoelectron spectroscopy (XPS), Raman spectrometer, atomic force microscopic (AFM) and dynamic contact angle analysis (DCA) were carried out to investigate CF reinforced composites. And test results demonstrated that the presence of Ag NPs and GO sheets increased the surface roughness and surface energy of CFs significantly. IFSS of CF/epoxy and the tensile strength of CFs were increased by 86.1% and 36.8%, respectively. Ag NPs filled in the cracks in CF effectively to enhance the tensile strength, while GO sheets improved the wettability of resin on CFs and formed mechanical interlocking between CFs and epoxy resin. These Ag NPs and GO sheets worked together in a ferocious synergy on the interface of CF and epoxy to cause the enhanced mechanical properties.

© 2017 Elsevier Ltd. All rights reserved.

1. Introduction

In recent decades, carbon fibers (CFs), which worked as an ideal reinforcing phase in polymer composites, have attracted tremendous attentions due to their low weight, high stiffness, excellent tensile strength and high thermal stability [1—3]. However, certain drawbacks of CFs/polymer composites, which are the poor wettability and weak adhesion between CF and matrix, limit their wide

applications [4,5]. And weak interfacial strength leads to deteriorating performance of composite materials. Therefore, enhancing the interfacial adhesive properties between CF and matrix such as epoxy via surface modification with various nanoscale materials is critical [6,7]. Graphene or graphene oxide (GO) has been demonstrated as an ideal candidate for selective reinforcement of fiber-matrix interface regions or hydrogels [8,9] owing to its outstanding thermal, electrical and mechanical performance [10—13]. The combination of CFs and graphene would help the stress transfers from weak matrix to strong fibers [14]. For example, the mechanical properties of graphene or GO reinforced CF/epoxy composites are enhanced dramatically [15]. However, the improvement of fiber tensile strength is relatively disappointing, for example, −9.8% in PBO fibers/epoxy composites [16], 7.9% in CF/

* Corresponding author.
** Corresponding author.
*** Corresponding author.
E-mail addresses: ydhuang.hit1@aliyun.com (Y. Huang), wangn02@foxmail.com (N. Wang), zguo10@utk.edu (Z. Guo).

epoxy composites [17] and 12.4% in CF/polyethersulfone composites [15].

Metal or metallic oxide nanoparticles were usually used to reinforce epoxy composites [18,19]. Metal nanoparticles have been also used to functionalize CFs, which exhibited greatly enhanced tensile strength [20], it was speculated that the metal nanoparticles could fill in the surface cracks of fibers and increase the radius of the crack tip to avoid the stress concentration. Among metal nanoparticles, Ag nanoparticles (Ag NPs) are popular due to their high electrical and thermal conductivities [21,22]. Besides, electrodeposition method with many advantages, for example, good uniformity, high efficiency, high yield, thickness controllable, binder-free and easy to scale up can be used to deposit metal, phosphors or catalysis coatings from a stable solution [23]. Analogously, electrophoretic deposition (EPD) is also a versatile technique that can be used to deposit any powdered solid (from micro- to nano-particles) from a stable suspension. Now EPD has been developed to deposit nanotube, graphene and graphene-based materials for field emitters or energy storage applications. However, to combine both nanoparticles and GO onto CFs has not been reported.

In this paper, we presented new Ag NPs and GO modified CF reinforcement to strengthen the mechanical property of CF/epoxy composites. Efficient electrophoretic deposition (EPD) and electrodeposition were carried out to deposit Ag NPs and GO onto the surface of CF layer by layer, respectively. Ag NPs and GO sheets were able to fill in the surface cracks on fibers and increase the wettability between matrix and fiber, respectively. Epoxy matrix was selected to evaluate the performance of CF reinforced composites due to its widespread use as engineering materials. Mechanical properties and surface properties of CFs with and without surface treatments were compared. It has been found that after modification, the novel two-layer reinforced CF was able to enhance IFSS of CF/epoxy, as well as CF tensile strength. Besides, this easy and efficient modification method could be helpful to industrial application of high-performance CF reinforcements.

2. Materials and methods

2.1. Materials

CFs (T700SC) was provided by Toray (Japan). GO was produced by oxidation of scaly graphite through modified Hummer's method [24,25]. Silver nitrate (AgNO₃) and poly (vinylpyrrolidone) (PVP Mn = 30,000) were supplied by Sigma-Aldrich. Hydrochloric acid (36−38%), concentrated sulfuric acid (95−98%), concentrated nitric acid (68%), isopropyl alcohol, potassium permanganate (KMnO₄) and magnesium nitrate hexahydrate (Mg(NO₃)₂·6H₂O) were provided by Sinopharm Chemical Reagent Co., Ltd. (Shanghai).

2.2. Experimental procedures

2.2.1. Electrodeposition, EPD and preparation of modified CFs/epoxy microdroplets

As-received CFs were firstly desized in refluxed acetone for 48 h, marked as untreated CF. Then, Ag NPs were prepared to fill in the surface cracks on fibers and improve the tensile strength of CF by electrodeposition. Briefly, an electrophoresis apparatus was connected with conductive substrates, the untreated CF bundle used as cathode, and a stainless steel tubing served as anode. AgNO₃ and PVP were used as support electrolyte. The concentration of AgNO₃ was 6 mmol L^{-1}, and the mole ratio of PVP to AgNO₃ in the electrolyte was 3:1. Electrodeposition was performed with the applied voltage (E) of 30 V, and the parallel arrangement with spacing (d) of 1 cm. After varying the deposition time of 10 s, 30 s, 60 s and 90 s,

the Ag-loaded CFs were cleaned with excess water, and let it in the air for 24 h, marked as CF/Ag-10, CF/Ag-30, CF/Ag-60 and CF/Ag-90, respectively. Subsequently, GO was deposited on the surface of CF/Ag-30 by EPD process. These GO sheets could increase the specific surface area of CF and stick into the matrix to enhance the mechanical interlocking. Briefly, EPD was performed within 200 mL electrophoretic ink, which was a mixture of GO (0.1 mg/mL) and Mg(NO₃)₂·6H₂O (0.1 mg/mL render the graphene sheets positively charged) ultrasonic-dispersed in isopropyl alcohol. After that, CF/Ag-30 was used as cathode, and stainless steel tubing was served as anode. EPD performed in condition of $d = 1$ cm, $E = 160$ V for 30 s, 60 s or 120 s, respectively. Then all the modified CFs were cleaned with excess water and isopropyl alcohol, and let them in air for 24 h. The resulted modified CFs are marked as CF/Ag/GO-30, CF/Ag/GO-60 and CF/Ag/GO-90, respectively. The scheme of preparation of CF/Ag/GO was shown in Fig. 1.

Resin microdroplets were mixed by epoxy resin and the hardener, which contains the WSR618 and methyl tetrahyelrophthalic anhydride (weight ratio 100:32), and then the mixture was applied on a single CF to form resin microdroplet. The curing process took place for 2 h at 90 °C, 2 h at 120 °C and 4 h at 150 °C. The prepared specimens were used to evaluate interfacial properties.

2.2.2. Characterizations of CFs

IFSS of CF and epoxy was assessed by micro-bond test via the interfacial evaluation equipment (FA620, Japan). The test was carried out by a moving trestle together with a single fiber at a displacement rate of 0.05 μm/s. Then the prepared specimens were tested and the maximum loads during the test were noted down. The IFSS was counted using Equation (1) [16].

$$IFSS = \frac{F}{\pi dl} \tag{1}$$

where F is the recorded maximum load, d is the diameter of CF, and l is the effective length of CF that embedded in the matrix.

SEM measurements of GO and modified CFs were performance (200FEG, Quanta FEI Inc. USA) used to access, by operating at 20 kV. Gold sputtering was applied before SEM observation to improve the conductivity for better imaging. TEM (Hitachi H-7650) was carried out to investigate the microstructures of GO and CF/Ag/GO, by operating at 200 kV accelerating voltage. AFM was carried out to examine the thickness of GO and the surface roughness (Ra) of different CFs, using NT-MDT Solver-P47H in the tapping mode of operation. The chemical compositions of CFs were analyzed quantitatively by XPS, using ESCALAB 220i-XLVG instrument at a monochromatic Al Kα source (energy 1486.6 eV). The chemical groups on CFs surface were measured by FTIR spectrum (Nicolet, Avatar360, USA) with the wavenumber range of 400–3600 cm^{-1}. Raman spectra were collected by Renishaw 2000 Raman spectrometer.

Monofilament tensile test was performed based on the ASTM

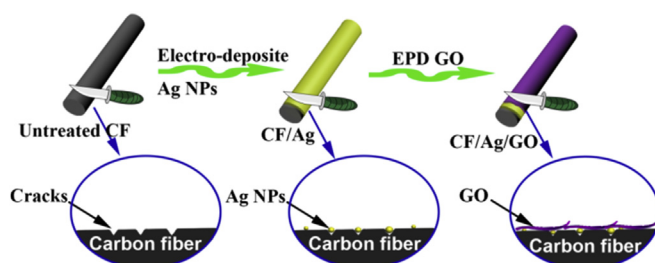**Fig. 1.** Schematic diagram of the procedure for the fabrication of CF/Ag/GO.

D3379-75 [26], where made on Instron 5566 at crosshead speed of 10 mm·min^{-1} and the gauge length of 20 mm. Effective data was collected and analyzed base on the Weibull statistical method [27].

Dynamic contact angle meter and tensiometer was carried out to access dynamic contact angle of CFs using DCAT21 Data-Physics Instruments. The liquids for test is deionized water (γ^d = 21.8 mN m^{-1}, γ = 72.8 mN m^{-1}) and diiodomethane (γ^d = 50.8 mN m^{-1}, γ = 50.8 mN m^{-1}) [28]. The surface energy (γ_f), polar component (γ_f^p) and dispersion component (γ_f^d) of the CFs were estimated by Equations (2) and (3) [2],:

$$\gamma_l(1 + \cos\theta) = 2\left(\gamma_l^p\gamma_f^p\right)^{1/2} + 2\left(\gamma_l^d\gamma_f^d\right)^{1/2} \qquad (2)$$

$$\gamma_f = \gamma_f^p + \gamma_f^d \qquad (3)$$

where θ, γ_l, γ_l^d and γ_l^p are the advancing contact angle, the surface tension of the test liquid, the dispersive component of γ_l, and the polar components of γ_l, respectively.

3. Results and discussion

3.1. The characterizations of GO sheets

Fig. 2a&b shows SEM and TEM micrographs of the obtained GO. GO shows flat and thin wrinkled structure which can be observed the transparent sheets in several micrometers. This unique wrinkled structure can greatly strengthen mechanical interlocking and stress transmission between modified CFs and matrix [29]. AFM micrograph exhibits that the thickness of the GO used in EPD is 1.41 ± 0.25 nm, as shown in Fig. 2c.

3.2. The effects of Ag and GO loadings

The loading content of Ag and GO on CF has effects on the mechanical properties of CF composites directly properties of [20]. Table 1 shows the Ag contents and single fiber tensile strength of Ag NPs-loaded CFs. The results suggest that Ag content and the tensile

strength increase as deposition time goes on at the beginning. When the deposition time exceeds 30 s, the single fiber tensile strength of CF/Ag becomes constant. Thus, 30 s is chosen as the best deposition time in this work and CF/Ag-30 is chosen for further deposition of GO.

As for the preparation of CF/Ag/GO, CF/Ag-30 is used as the working electrode under different EPD time. Fig. 3a–c shows the surface morphology of CF/Ag/GO-30, CF/Ag/GO-60 and CF/Ag/GO-120, respectively. This proves that the load amount of GO increases with the EPD time. When EPD time is 120 s, CF/Ag/GO-120 has a heavy layer and the GO sheets agglomerate on the CF surface, which facilitates the stress concentration location in the interfaces. Table 2 describes the IFSS and single fiber tensile strength of CF/Ag/GO prepared with different EPD time intervals. The results demonstrate that after the EPD of GO, IFSS of CF/Ag/GO improves sharply while the tensile strength slightly increases. This is because the presence of GO increased the surface roughness and the number of active functional groups. GO could enhance wettability, and then enhance the interfacial interaction of CF and epoxy [20]. It is shown that while the deposition time increases, the IFSS value increases first and then decreases. As the deposition time increases, the amount of GO deposited on CF grows and further the wettability and mechanical interlocking between CF and epoxy increase. However, when the deposition time is over 60 s, the IFSS value starts to decrease, this is because that the weak van der Waals interaction among GO sheets lead to the interface failure in the heavy layer of the GO sheets [30]. Therefore, the best EPD time is 60 s.

3.3. Surface morphologies of CFs

The morphologic characterization (Fig. 4) shows the surface morphology changes of untreated CFs and modified CFs. The SEM image of Fig. 4a reveals that untreated CF surface is neat and smooth. After deposition of Ag NPs, the surface morphology of CF/Ag-30 (Fig. 4b) does not show obvious changes because the nano-sized Ag particles are hard to be observed under low magnification. The smooth surface of CF roughens up in high-magnification
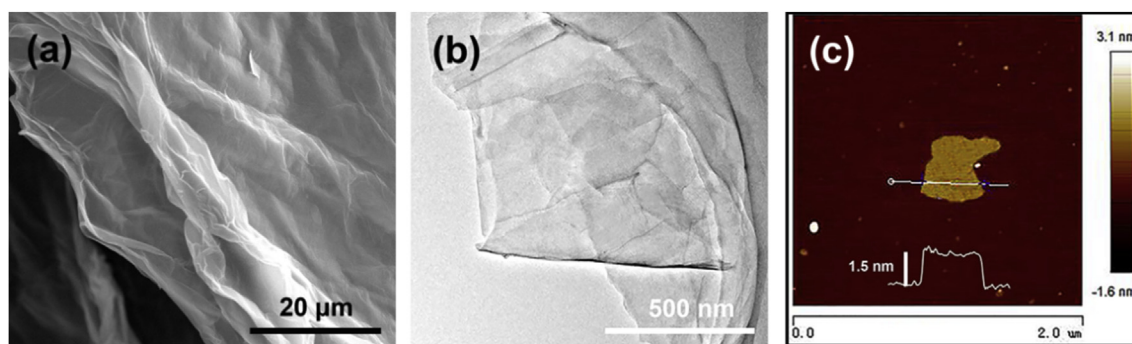

Fig. 2. Morphology of GO sheets. (a) SEM image of GO, (b) TEM image of a GO film, and (c) AFM image of a GO sheet. The white line inset represents the corresponding height profile of GO.

Table 1
Ag contents and single fiber tensile strength of Ag NPs-loaded CFs in different deposition time.

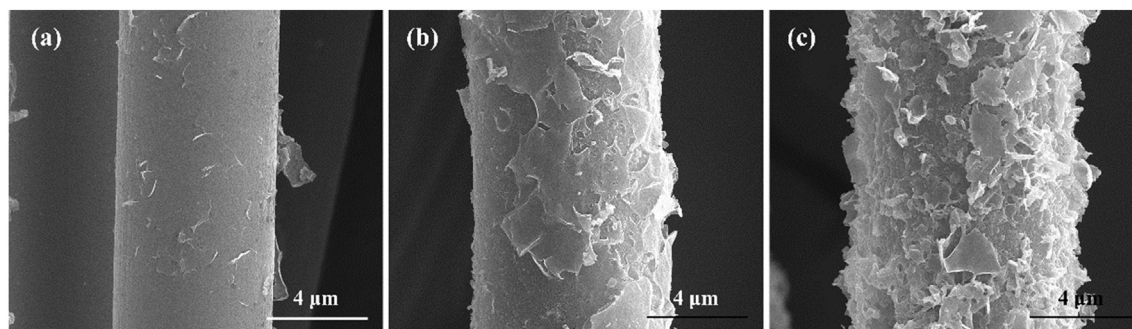| Samples	Time (s)	Ag (%)	Weibull shape parameter (m)	Tensile strength (GPa)
Untreated CF	0	0	4.65	4.54 ± 0.30
CF/Ag-10	10	0.75	5.02	4.98 ± 0.37
CF/Ag-30	30	1.82	5.78	5.76 ± 0.42
CF/Ag-60	60	3.36	5.81	5.79 ± 0.45
CF/Ag-90	90	5.21	5.82	5.81 ± 0.51

Fig. 3. SEM images of (a) CF/Ag/GO-30, (b) CF/Ag/GO-60 and (c) CF/Ag/GO-120.

Table 2
IFSS and single fiber tensile strength of CF/Ag/GO in different EPD time.

Samples	Time (s)	IFSS (MPa)	Weibull shape parameter (m)	Tensile strength (GPa)
Untreated CF	0	46.8 ± 4.91	4.65	4.54 ± 0.30
CF/Ag-30	0	73.6 ± 5.52	5.78	5.76 ± 0.42
CF/Ag/GO-30	30	83.5 ± 7.11	5.92	5.91 ± 0.51
CF/Ag/GO-60	60	87.1 ± 7.84	6.34	6.21 ± 0.57
CF/Ag/GO-120	120	84.2 ± 8.42	6.35	6.23 ± 0.68

image in Fig. 4c. The Ag NPs are well dispersed on the surface of CF/Ag-30 and the particle size appears to be pretty uniform. On the other hand, after the EPD of GO, a great change emerges on the surface morphology of CF/Ag/GO-60, as shown in Fig. 4d–f. GO sheets in different sizes are observed to be attached firmly to the CF/Ag/GO-60, forming a unique hierarchical structure. In addition, the Ag NPs can be observed under the GO sheets clearly, indicating the improved stability of Ag NPs by the EPD of GO. This new hybrid structure is expected to be beneficial to enhance interfacial property between CF and matrix. The mechanical properties of composites can be obviously enhanced by addition of nano carbon materials into composites, such as nanotubes [31,32] or graphene.

AFM images of different samples (Fig. 5a–c) show varied surface roughness along with SEM images. For the untreated CF, the surface looks smoothly and neatly. And the practical production of CF has contributed to several narrow grooves. The surface roughness (Ra) value of untreated CF is 50.2 nm. The higher surface roughness (Ra = 96 nm) of CF/Ag-30 (Fig. 5b) is due to the deposition of a large number of Ag NPs. After deposition of GO, large quantities of GO sheets are attached to CF/Ag/GO-60 (Fig. 5c) leads to the highest roughness (Ra = 197 nm). The increased roughness is good for mechanical interlocking of CF and epoxy.

To explore the interfacial structure among Ag NPs, GO sheets and CF, TEM was used to observe this hierarchical structure. The
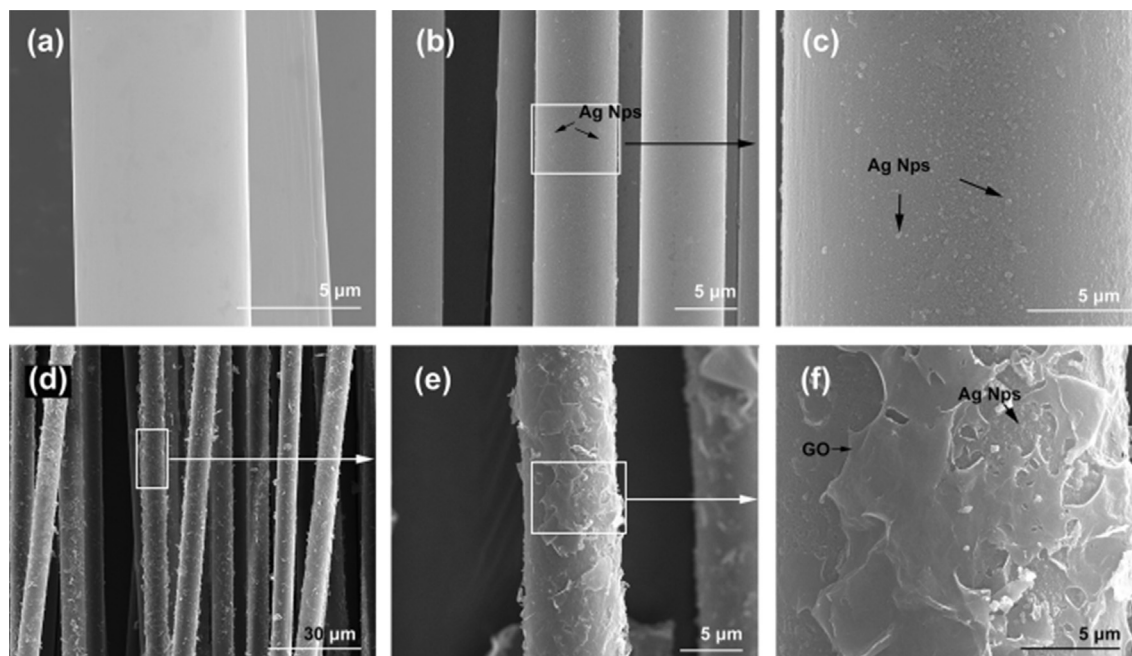

Fig. 4. SEM images of (a) untreated CF, (b,c) CF/Ag-30, (c–f) CF/Ag/GO-60.
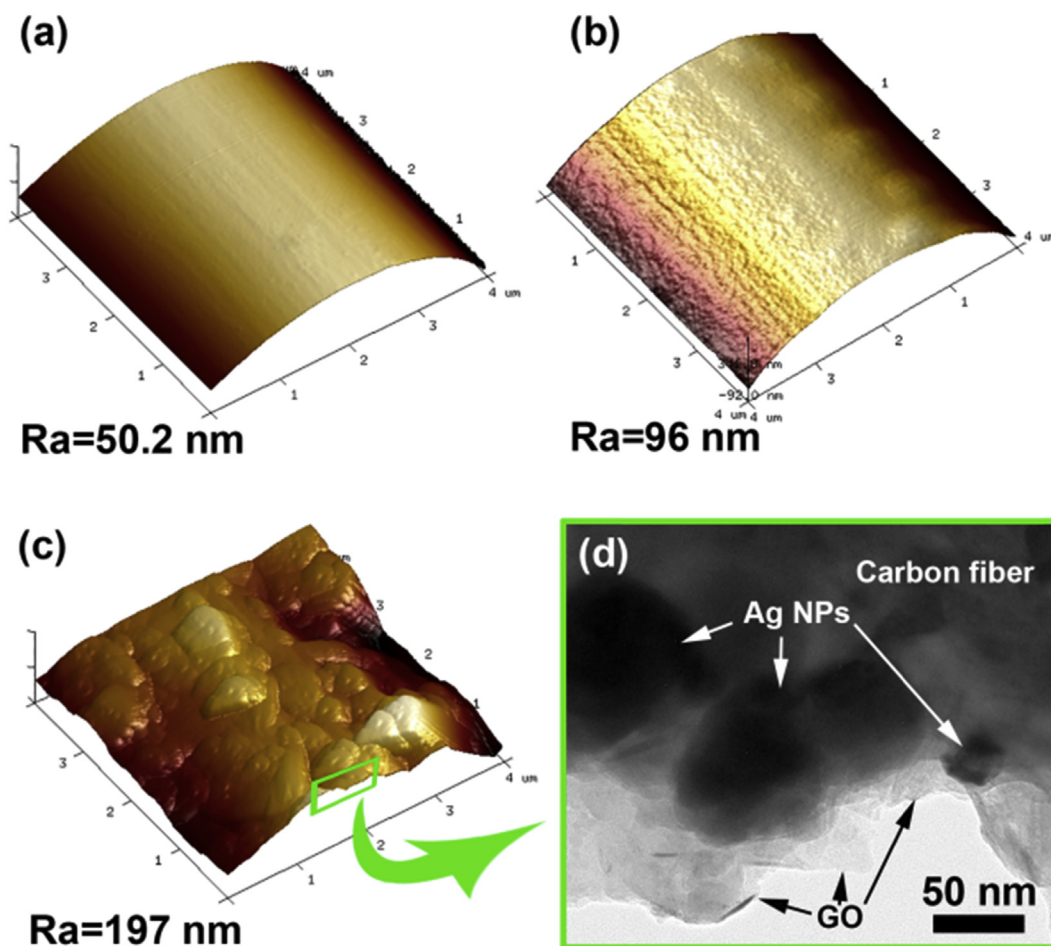
Fig. 5. AFM images of (a) untreated CF, (b) CF/Ag-30, (c) CF/Ag/GO-60 and TEM image of cross-section of (d) CF/Ag/GO-60. TEM micrograph showing the nanocomposite structure near the fiber/matrix interface.

cross section of CF/Ag/GO-60 (Fig. 5d), thin GO sheets can be seen on the surface of CF. Some spherical particles (about 30–70 nm in diameter) appear between the GO sheets and CF, which are found to be Ag NPs. This proves that new interface structure has been formed on the CF/Ag/GO. That is to say that both Ag NPs and GO are deposited on CF surface successfully and this hierarchical structure might be beneficial to fill the defects and enhance the interfacial strength [33].

3.4. Surface characteristics of CF

The element composition of CFs and the successful deposition of Ag NPs and GO were corroborated using XPS. Fig. 6a reveals the wide-scan XPS spectra of different samples, while Table 3 shows the calculated results. Silver element can be found on CF/Ag-30, suggesting that the silver ions have been converted to metallic silver during the deposition process (small peaks at 368.32 eV and 374.27 eV match Ag $3d_{5/2}$ and Ag $3d_{3/2}$). Compared with the untreated CF and CF/Ag-30, the CF/Ag/GO-60 has the highest oxygen content, indicating that GO sheets, which contain large amounts of active functional groups, have been successfully deposited on CF surface. Moreover, the surface silver content of CF/Ag/GO-60 decreases from 0.61% to 0.23%, because the Ag NPs are covered by GO sheets.

The C1s spectra of GO are fitted into four peaks (Fig. 6) to know the types of functional groups on GO [34]. The four peaks centered at 284.6 eV (peak I) corresponding to graphitic carbon; 286.1–286.3 eV (peak II) corresponding to epoxy phenolic and alcoholic groups [35]; 287.3–287.6 eV (peak III) corresponding to carbonyl or quinone groups and 288.4–288.9 eV (peak IV) corresponding to carboxyl or ester groups. It is expected that the carboxyl, epoxy and hydroxyl groups of GO sheets increase wettability between CF and polar resin. While compared with the C1s spectra of untreated CF and CF/Ag-30, the C 1s spectrum of CF/Ag/GO-60 shows more oxygen related groups. The increased peak areas of hydroxyl and carboxyl are observed in Fig. 6d. These oxygenic groups are beneficial for increasing the wettability between CFs and resin.

The studies of FTIR (Fig. 7a) showed differences between spectra of untreated CF and CF/Ag/GO-60. Compared with untreated CF, new features on the spectrum of CF/Ag/GO-60 at 1050 and 1240 cm^{-1} are assigned to the stretching vibration of C-O-C [36]. The new peak at 1408 cm^{-1} is related to COO- stretching modes of ester group. The new features at 1620 and 1730 cm^{-1} are due to -COOH and C=O stretching modes of carbonyl group. The peak at 3350 cm^{-1} is assigned to the stretching vibration of -OH. This proves that GO sheets is deposited successfully on CFs.

Raman spectroscopy (Fig. 7b) is adopted to analyze the structures of CF surface. In similar spectra, two Raman bands are observed around 1333 and 1590 cm^{-1} in both untreated CF and CF/Ag/GO, which are assigned to the G and D bands that correspond to the E2g mode and A1g mode [37], respectively. The integral area
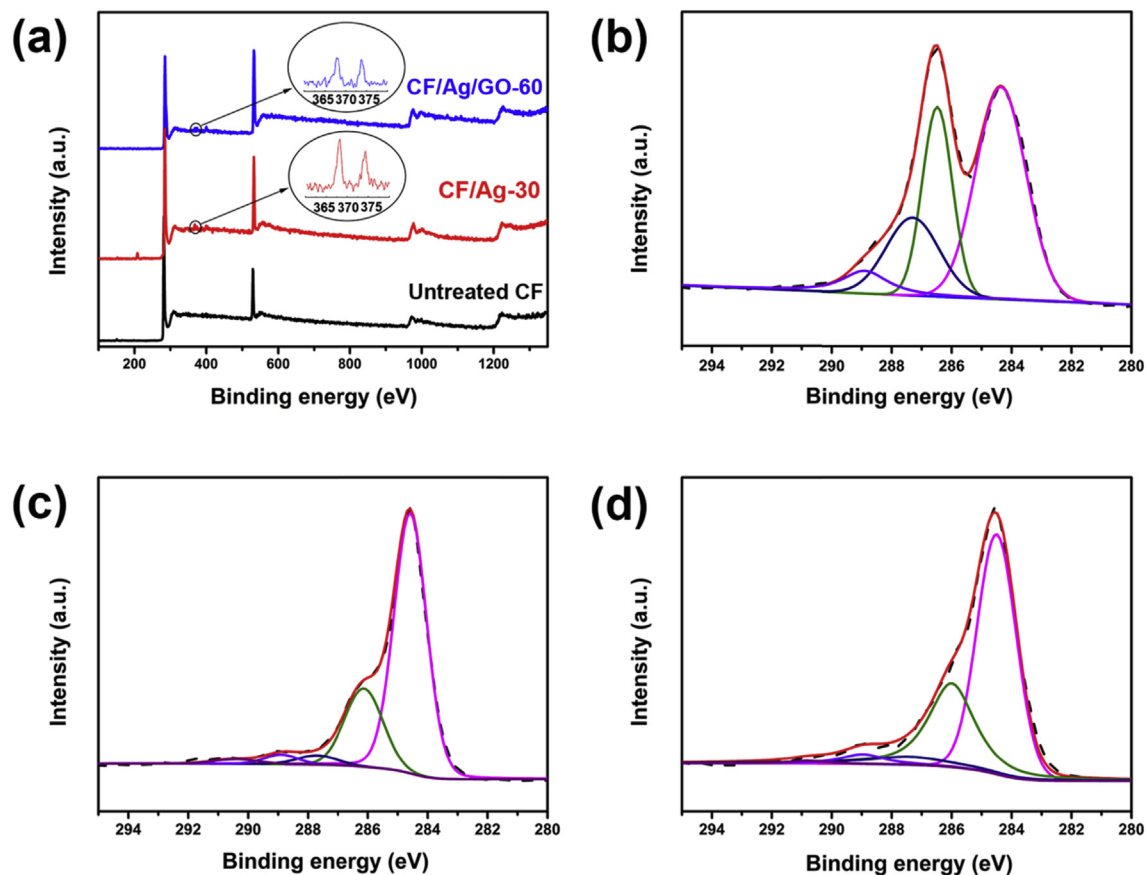
Fig. 6. (a) Wide-scan XPS spectra of different CF samples and C 1s high-resolution XPS element spectra of (b) GO, (c) untreated CF and (d) CF/Ag/GO-60.

Table 3
Surface element compositions of the samples.

Samples	Element contents (%)		
	C (%)	O (%)	Ag (%)
Untreated CF	87.37	12.63	0
CF/Ag-30	86.71	12.68	0.61
CF/Ag/GO-60	75.11	25.66	0.23

ratio of D/G bands (I_D/I_G) explains the crystalline order of carbonaceous materials. I_D/I_G of GO is 1.43 due to defect or disorder of crystalline surface structure. After deposition of GO, I_D/I_G of CF sample increases from 0.96 (untreated CF) to 1.07(CF/Ag/GO-60). This indicates that GO, which possesses more defect or disorder, covered the surface of CF [38]. Therefore, the CF/Ag/GO-60 shows a low graphitic crystalline surface structure. The increased number of structural defects and surface functional groups on the surface of CF/Ag/GO-60 is beneficial for increasing the surface energy.

3.5. Wettability of CF

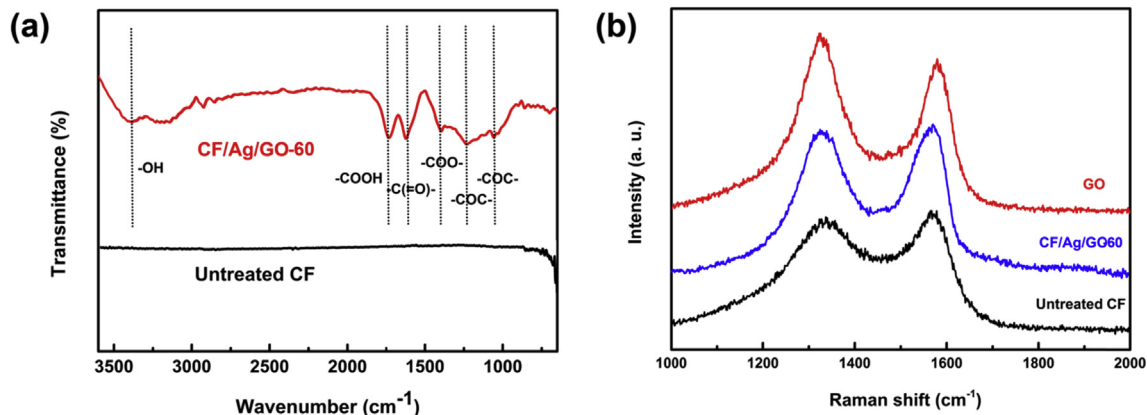Advancing dynamic contact angle analysis was used to evaluate

Fig. 7. FT-IR spectra (a) and Raman spectra (b) of different samples.

the surface energy of CFs. As shown in Fig. 8 a&b, the contact angles of water decrease after the deposition of Ag NPs and GO sheets, as well as diiodomethane. After the deposition of Ag NPs, the surface energy γ of CF increases from 40.8 mJ m^{-2} to 44 mJ m^{-2}. And the surface energy γ of CF/Ag/GO-60 is 52 mJ m^{-2}. As for the CF/Ag-30, the increased roughness gives rise to the increase of dispersive component γ^d of surface energy [39]. As for the CF/Ag/GO-60, large amount of active functional groups CF/Ag/GO-60 is beneficial to the increase of polar component γ^p of surface energy. After EPD of GO, the surface topography changes greatly compared to untreated CF and CF/Ag-30, which is good for the improvement of dispersive component γ^d. In summary, new hybrid reinforced CF has a better interfacial wettability due to the surface topography and active functional groups.

3.6. Tensile strength of CF

The data of monofilament tensile tests are analyzed using the Weibull distribution function [28]. As shown in Table 2, tensile strength of CF/Ag-30 and CF/Ag/GO-60 is higher than that untreated one. As for CF/Ag-30, the Ag NPs can fill the surface cracks on the CFs and effectively weaken the stress intensity at the crack tips. As for the CF/Ag/GO-60, the deposition of GO changes the surface morphologies of CF greatly, and the tensile strength of CF/Ag/GO-60 is the highest among all the samples. It is considered that the addition of GO sheets with outstanding mechanical property is the result of bridging the surface microcracks [13]. Moreover, the increase of tensile strength of CF is much higher than those reported in previous works [14–16]. Thus, it can be concluded that the hybrid reinforced CF/Ag/GO-60 has its practical significance for preparing high performance fiber/matrix composites.

3.7. IFSS of fiber-epoxy composites

The fiber-epoxy matrix interfacial bond was assessed by testing the microbond specimens. The IFSS values of CF/epoxy are provided in Fig. 8c. After the deposition of Ag NPs, IFSS of CF/epoxy increases from 46.8 MPa (untreated CF) to 73.6 MPa (CF/Ag-30). The presence of Ag NPs improves the surface roughness of the CF (Fig. 5b). The rough surfaces can greatly strengthen the mechanical interlocking between CF and matrix, which had been reported [40,41]. After the EPD of GO, the IFSS of CF/Ag/GO-60 increases to 87.1 MPa. The deposition of GO introduces active functional groups and roughs surface, which raise the wettability and interfacial interaction between CF and epoxy [33]. Moreover, the deposited GO results in an enlarged specific surface area, which is beneficial to consume destructive energy and prevents the fiber from being pulled out from the resin matrix.

Fig. 9a–c depicts the surface morphology of CFs debonded from the epoxy. For the untreated CF (Fig. 9a), few epoxy fragments remains on the debonded fiber surface, indicating poor interfacial properties because weak van der Waals force. For CF/Ag-30, more epoxy debris still adhered on the CF (Fig. 9b), and there are many scratches on the surface the fiber due to the movement of Ag NPs with the debonding of epoxy. Fig. 9e&f shows the EDS results of (e) CF/Ag-30 and (f) CF/Ag/GO-60 after debonding from epoxy matrix. They demonstrate the Ag peaks in the EDS spectrum taken from areas outlined in black in Fig. 9b. This indicates that Ag NPs filled the cracks and microholes on the CF, and lefts on the surface of CF/Ag-30. Meanwhile, it is found that a large number of epoxy still keeps on the debonded CF/Ag/GO-60, as shown in Fig. 9c. It suggests that interfacial interaction of fiber and matrix is stronger than cohesive energy of resin matrix, and cohesive failure occurs in the interface between epoxy resin and CF/Ag/GO-60. Furthermore, Some Ag NPs still adhere to the surface of CF/Ag/GO-60 and Ag NPs do not move with epoxy droplets (demonstrates by EDS of Fig. 9f). These remaining Ag NPs can strengthen mechanical interlocking between CF and GO sheets. Additionally, some GO sheets (marks by arrows) can be found on debonded fiber surface, indicating the strong interaction between GO and CF.

The variations of IFSS can be explained by different interfacial failure modes of CF/epoxy microbond. In general, there are two interfacial failure modes of fiber/resin microbond, adhesive failure and cohesive failure, as shown in Fig. 9d. For the untreated CF, few
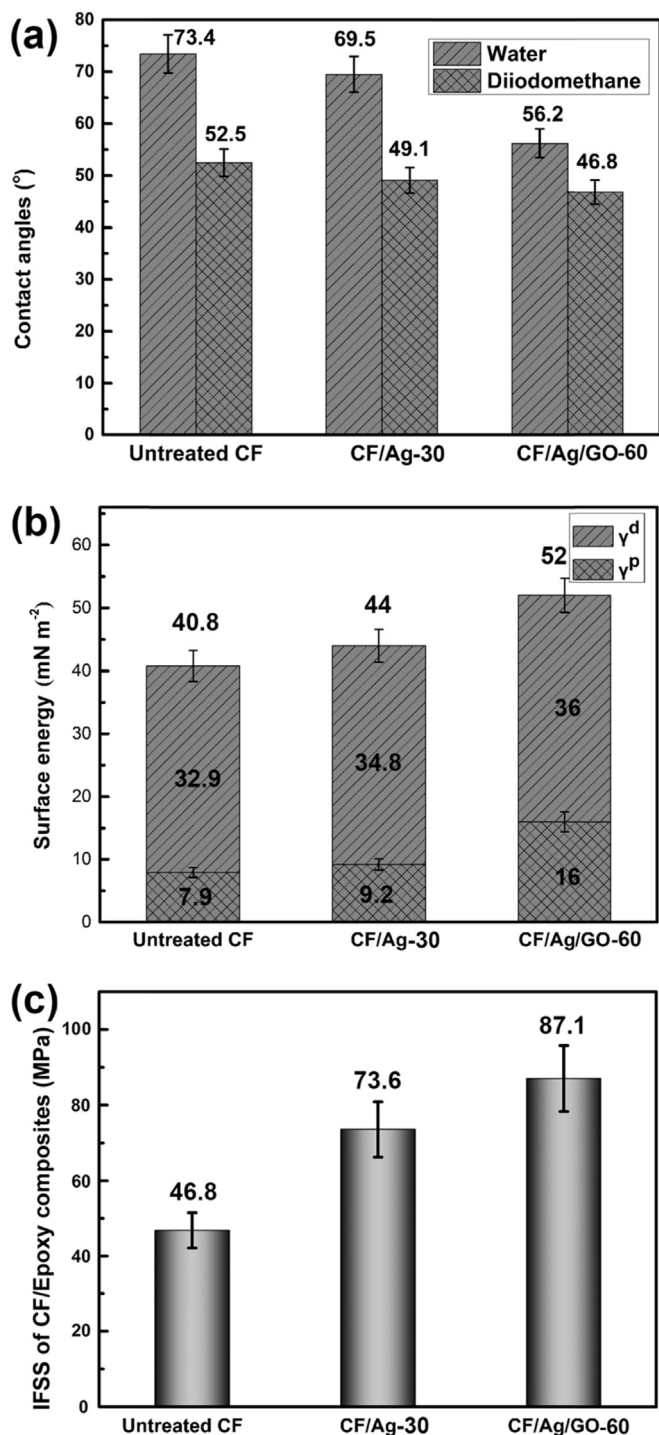

Fig. 8. Surface properties and mechanical performance of CFs: (a) Contact angles, (b) surface energy and (c) IFSS of the CF/epoxy microbond.
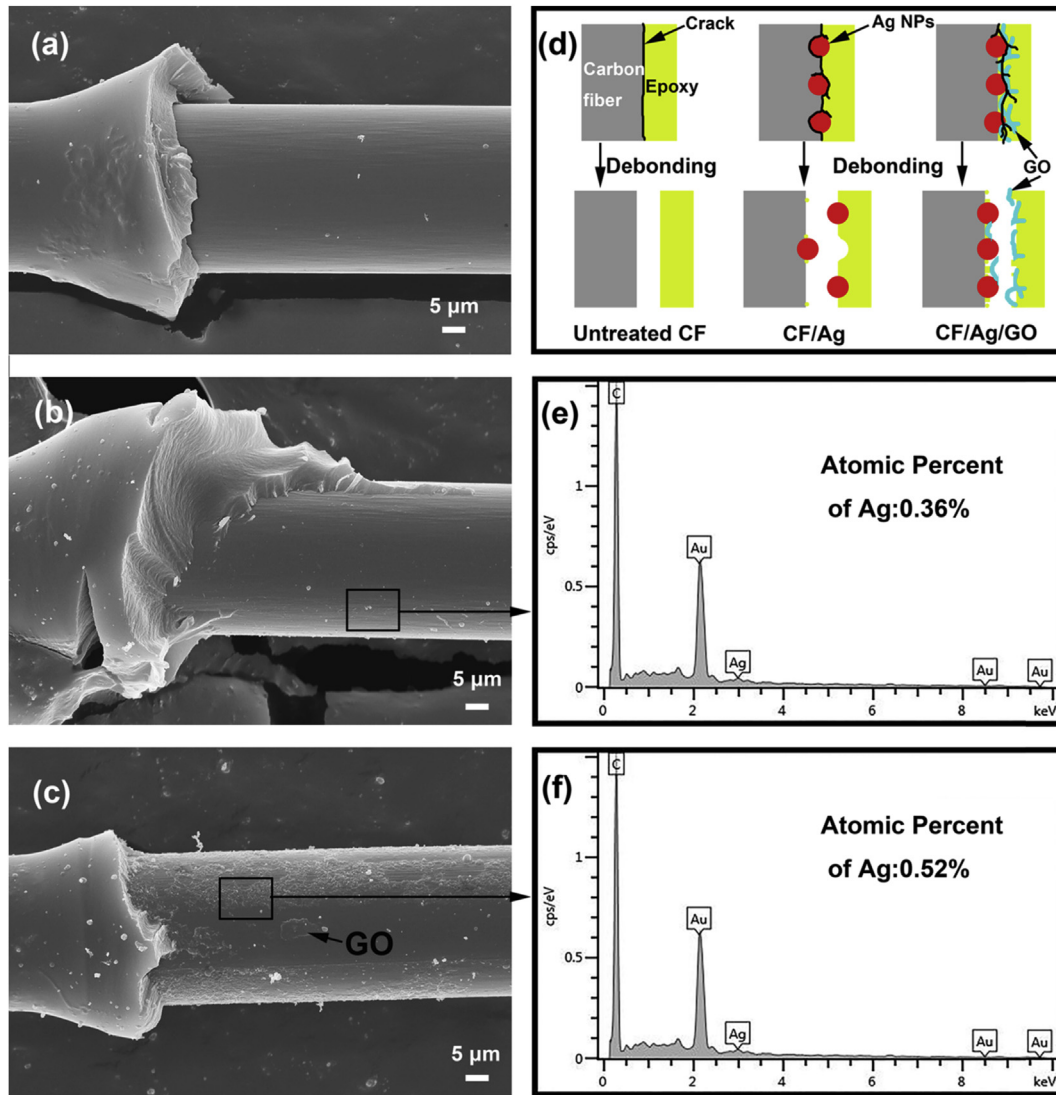
Fig. 9. SEM images of (a) untreated CF, (b) CF/Ag and (c) CF/Ag/GO after debonding from epoxy matrix. (d) Sketch of failure mode of samples. For untreated CF and CF/Ag, a small amount of epoxy matrix keeps on the surface of fibers, belonging to an adhesive failure; while for the CF/Ag/GO that more epoxy matrix keeps on the surface of fiber, belonging to a cohesive failure. And EDS results of (e) CF/Ag-30 and (f) CF/Ag/GO-60 after debonding from epoxy matrix.

epoxy keeps on fiber surface after debonding, the failure behavior mainly belongs to adhesive failure [29]. For the CF/Ag, the weak interaction is Van der Waals force, which leads to the interfacial failure occurs on the interphase between CF and Ag NPs, thus, the failure mode also belongs to adhesive failure [42]. Moreover, the content of Ag NPs of CF/Ag surface (0.36%) decreases, as shown in Fig. 9e Because some Ag NPs are deboned together with the epoxy (Fig. 9b). For the CF/Ag/GO, a large number of remain epoxy remains on the fiber surface (Fig. 9c), that is to say the interfacial failure occur in the epoxy matrix and transfer to the dominant cohesive failure. According to the above analys, it can be concluded that when the interfacial bond is strong enough (the IFSS is high enough), the failure mode would transfer to cohesive failure.

4. Conclusion

In this study, Ag NPs and GO sheets have been uniformly deposited on the CF trying to inprove IFSS of CF reinforced epoxy composites, as well as tensile strength of CF simultaneously. Meantime, IFSS of CF/epoxy composites increased from 46.8 MPa to 87.1 MPa, and the tensile strength of CF changed from 4.54 GPa to 6.21 GPa. For CF/Ag/GO-60, the IFSS of CF/epoxy enhanced by 86.1% and the tensile strength was improved by 36.8%. This is because that Ag NPs acting as "filler" are imbedded into the surface defects of fiber to modify the surface cracks. On the other hand, the deposited GO nanosheets increase the surface roughness and surface energy caused by introducing more functional groups. Moreover, this method is very simple with only 90 s to finish the deposition. In addition, in this new type of reinforcement, Ag NPs and GO sheets worked together in a strong synergy on the surfaces of CF, which effectively increases the interfacial properties of the resulting composites and the tensile strength of CF, simultaneously. This efficient method could be widely used in multifunctional and scalable fabrication of high-performance CFs for aerospace and automotive industries.

References

[1] M.S. Islam, Y. Deng, L. Tong, S.N. Faisal, A.K. Roy, V.G. Gomes, et al., Grafting carbon nanotubes directly onto carbon fibers for superior mechanical stability: towards next generation aerospace composites and energy storage applications, Carbon 96 (2016) 701—710.

[2] M. Martin-Gallego, R. Verdejo, M.A. Lopez-Manchado, M. Sangermano, High performance nat- ural rubber composites with a hierarchical reinforcement structure of carbon nano- tube modified natural fibers, Polymer 52 (2011) 4664—4669.

[3] D.W. Jiang, L. Liu, J. Long, L.X. Xing, Y.D. Huang, Z.H. Guo, et al., Reinforced unsaturated polyester composites by chemically grafting amino-POSS onto carbon fibers with active double spiral structural spiralphosphodichloror, Compos. Sci. Technol. 100 (2014) 158—165.

[4] X.Z. Tang, B. Yu, R.V. Hansen, X. Chen, X. Hu, Grafting low contents of branched polyethylenimine onto carbon fibers to effectively improve their interfacial shear strength with an epoxy matrix, J. Adv. Mater. Interfaces 2 (2015) 1—7.

[5] M.A. Montes-Moran, R.J. Young, Raman spectroscopy study of HM carbon fibres: effect of plasma treatment on the interfacial properties of single fibre/epoxy composites. Part I: fibre characterization, Carbon 40 (2002) 845—855.

[6] Y. Ma, Y. Guo, Y. Fu, Q. Shao, T. Wu, et al., Porous lignin based poly (acrylic acid)/organo-montmorillonite nanocomposites: swelling behaviors and rapid removal of Pb (II) ions, Polymer 128 (2017) 12—23.

[7] Z. Wu, S. Gao, L. Chen, D. Jiang, Q. Shao, Z. Guo, et al., Electrically insulated epoxy nanocomposites reinforced with synergistic core-shell SiO_2@MWCNTs and montmorillonite bifillers, Macromol. Chem. Phys. (2017), https://doi.org/10.1002/macp.201700357 (in press).

[8] X.Q. Yan, Q. Chen, L. Zhu, H. Chen, D. Wei, F. Chen, Z. Tang, J. Yang, J. Zheng, High strength and self-healable gelatin/polyacrylamide double network hydrogels, J. Mater. Chem. B 5 (2017) 7683—7691.

[9] Z.Q. Tang, F. Chen, Q. Chen, L. Zhu, X.Q. Yan, H. Chen, B.P. Ren, J. Yang, G. Qin, J. Zheng, The energy dissipation and Mullins effect of tough polymer/graphene oxide hybrid nanocomposite hydrogels, Polym. Chem. 8 (2017) 4659—4672.

[10] Z.S. Wu, S.F. Pei, B.L. Liu, H.M. Cheng, Field emission of single-layer graphene films prepared by electrophoretic deposition, Adv. Mater. 21 (2009) 1756—1760.

[11] T. Liu, K. Yu, L. Gao, H. Chen, N. Wang, Z. Guo, et al., Graphene quantum dots decorated $SrRuO_3$ mesoporous film as an efficient counter electrode for high-performance dye-sensitized solar cells, J. Mater. Chem. A 5 (2017) 17848—17855.

[12] (a) X.G. Li, G.B. McKenna, G. Miquelard-Garnier, A. Guinault, C. Sollogoub, G. Regnier, et al., Forced assembly by multilayer coextrusion to create oriented graphene reinforced polymer nanocomposites, Polymer 55 (2014) 248—257;
(b) J. Zhang, Y. Liang, X. Wang, et al., Strengthened epoxy resin with hyperbranched polyamine-ester anchored graphene oxide via novel phase transfer approach, Adv. Compos. Hybrid Mater. (2017), https://doi.org/10.1007/s42114-017-0007-0. https://doi.org/10.1007/s42114-017-0007-0 (in press).

[13] T. Liu, K. Yu, L. Gao, H. Chen, N. Wang, L. Hao, et al., Graphene quantum dots decorated $SrRuO_3$ mesoporous film as an efficient counter electrode for high-performance dye-sensitized solar cells, J. Mater. Chem. A 5 (2017) 17848—17855.

[14] X.Q. Zhang, X.Y. Fan, Interfacial microstructure and properties of carbon fiber composites modified with graphene oxide, ACS Appl. Mater. Inter 4 (2012) 1543—1552.

[15] F. Li, Y. Liu, C.B. Qu, S.Y. Fu, Enhanced mechanical properties of short carbon fiber reinforced polyethersulfone composites by graphene oxide coating, Polymer 59 (2015) 155—165.

[16] L. Chen, F. Wei, L. Liu, W. Cheng, Z. Hu, Y.D. Huang, Grafting of silane and graphene oxide onto PBO fibers: multifunctional interphase for fiber/polymer matrix composites with simultaneously improved interfacial and atomic oxygen resistant properties, Compos. Sci. Technol. 106 (2015) 32—38.

[17] R.L. Zhang, B. Gao, Q.H. Ma, L. Liu, Directly grafting graphene oxide onto carbon fiber and the effect on the mechanical properties of carbon fiber composites, Mater. Des. 93 (2016) 364—369.

[18] C.B. Liang, P. Song, H.B. Gu, C. Ma, Y.Q. Guo, H.Y. Zhang, X.J. Xu, Q.Y. Zhang, J.W. Gu, Nanopolydopamine coupled fluorescent nanozinc oxide reinforced epoxy nanocomposites, Compos. Part A 102 (2017) 126—136.

[19] J. Guo, H.X. Song, H. Liu, C.J. Luo, Ding T. RenYR, M.A. Khan, D.P. Young, Xinyu Liu, X. Zhang, J. Kong, Z.H. Guo, Polypyrrole-interface-functionalized nano-magnetite epoxy nanocomposites as electromagnetic wave absorbers with enhanced flame retardancy, J. Mater. Chem. C 5 (2017) 5334—5344.

[20] C.F. Wang, J. Li, S.F. Sun, Y.D. Huang, Controlled growth of silver nanoparticles on carbon fibers for reinforcement of both tensile and interfacial strength, RSC Adv. 6 (2016) 14016—14026.

[21] M. Guo, X. Yi, G. Liu, L. Liu, Simultaneously increasing the electrical conductivity and fracture toughness of carbon-fiber composites by using silver nanowires-loaded interleaves, Compos. Sci. Technol. 97 (2014) 27—33.

[22] K. Sun, P. Xie, Z. Wang, T. Su, Q. Shao, J. Ryu, et al., Flexible polydimethylsiloxane/multi-walled carbon nanotubes membranous metacomposites with negative permittivity, Polymer 125 (2017) 50—57.

[23] S.Y. Huang, G.P. Wu, S.C. Zhang, C.X. Lu, Electrophoretic deposition and thermal annealing of a graphene oxide thin film on carbon fiber surfaces, Carbon 52 (2013) 605—620.

[24] C.F. Wang, J. Li, Y.D. Huang, Electrophoretic deposition of graphene oxide on continuous carbon fibers for reinforcement of both tensile and interfacial strength, Compos. Sci. Technol. 135 (2016) 46—53.

[25] V.R. Silvia, M.D. Juan, Tascon. Preparation of graphene dispersions and graphene-polymer composites in organic media, J. Mate. Chem. 19 (2009) 3591—3593.

[26] ASTM D3379-75, Standard Test Method for Tensile Strength and Young's Modulus for High-modulus Single-filament Materials, 1989.

[27] W. Weibull, A statistical distribution function of wide applicability, J. Appl. Mech. 18 (1951) 293—297.

[28] T. Darmanin, F. Guittard, Homogeneous growth of conducting polymer nanofibers by electrodeposition for superhydrophobic and superoleophilic stainless steel meshes, RSC Adv. 4 (2014) 50401—50405.

[29] Y. Li, Q. Peng, X. He, P. Hu, C. Wang, H. Lv, Synthesis and characterization of a new hierarchical reinforcement by chemically grafting graphene oxide onto carbon fibers, J. Mater. Chem. 22 (2012) 18748—18752.

[30] X. Shen, X. Pei, Y. Liu, S. Fu, Tribological performance of carbon nanotube-graphene oxide hybrid/epoxy composites, Compos. Part B 57 (2014) 120—125.

[31] S.S. Zeng, C. Reyes, J.J. Liu, P.A. Rodgers, Samuel H. Wentworth, L. Sun, Facile hydroxylation of halloysite nanotubes for epoxy nanocomposite applications, Polymer 55 (2014) 6519—6528.

[32] L.Y. Sun, G.L. Warren, D. Davis, H.J. Sue, Nylon toughened epoxy/SWCNT composites, J. Mater. Sci. 46 (2011) 207—214.

[33] J. Chen, D. Zhao, H. Ge, Modifying glass fibers with graphene oxide: towards high-performance polymer composites, Compos. Sci. Technol. 97 (2014) 41—45.

[34] Q. Peng, X. He, Y. Li, C. Wang, R. Wang, P. Hu, Y. Yan, T. Sritharan, Chemically and uniformly grafting carbon nanotubes onto carbon fibers by poly(amido-amine) for enhancing interfacial strength in carbon fiber composites, J. Mater. Chem. 22 (2012) 5928—5931.

[35] J. Zhang, H. Yang, G. Shen, P. Cheng, S. Guo, Reduction of graphene oxide via L-ascorbic acid, Chem. Commun. 46 (2010) 1112—1114.

[36] X. Shen, L. Meng, Z. Yan, C. Sun, H. Xiao, Improved cryogenic interlaminar shear strength of glass fabric/epoxy composites by graphene oxide, Compos. Part B 73 (2015) 126—131.

[37] G. Tang, Z. Jiang, X. Li, H. Zhang, S. Hong, Z. Yu, Electrically conductive rubbery epoxy/diamine-functionalized graphene nanocomposites with improved mechanical properties, Compos. Part B 67 (2014) 564—570.

[38] S. Wang, Z.H. Chen, W.J. Ma, Q.S. Ma, Influence of heat treatment on physical-chemical properties of PAN-based carbon fiber, Ceram. Int. 32 (2006) 291—295.

[39] X. Yang, Z. Wang, M. Xu, R. Zhao, X. Liu, Strengthened magnetic epoxy nanocomposites with protruding nanoparticles on the graphene nanosheets, Mater. Des. 44 (2013) 74—80.

[40] X. Zhang, O. Alloul, Q.L. He, J.H. Zhu, M.J. Verde, Z.H. Guo, Epoxy/graphene platelets nanocomposites with two levels of interface strength, Polymer 54 (2013) 3594—3604.

[41] I. Zaman, T.T. Phan, H.C. Kuan, Q.S. Meng, L.T.B. La, L. Luong, Grafting of polyhedral oligomeric silsesquioxanes on a carbon fiber surface: novel coupling agents for fiber/polymer matrix composites, Polymer 52 (2011) 1603—1611.

[42] F. Zhao, Y.D. Huang, Grafting of polyhedral oligomeric silsesquioxanes on a carbon fiber surface: novel coupling agents for fiber/polymer matrix composites, J. Mater. Chem. 21 (2011) 3695—3703.